RSC Advances

Conductive Hybrid Carbon Nanotube (CNT)-polythiophene coatings for Innovative Auditory Neuron-Multi-Electrode Array Interfacing

Journal:	*RSC Advances*
Manuscript ID	RA-ART-12-2015-027642.R1
Article Type:	Paper
Date Submitted by the Author:	05-Apr-2016

Complete List of Authors:	Ostrovsky, Stella; Bar-Ilan University, Institute of Nanotechnology & Advanced Materials & Department of Chemistry Hahnewald, Stefan; University of Bern, Inner Ear Research, Department of Clinical Research Kiran, Raphael; MED-EL Elektromedizinische Geräte GmbH Mistrik, Pavel; MED-EL Elektromedizinische Geräte GmbH Hessler, Roland; MED-EL Elektromedizinische Geräte GmbH Tscherter, Anne; University of Bern, Physiology Senn, Pascal; University of Bern, Inner Ear Research, Department of Clinical Research; University Hospital of Geneva (HUG), Switzerland , Department of Clinical Neurosciences, Service of Otorhinolaryngology, Head & Neck Surgery, Kim, Jinsang; University of Michigan, Materials Science and Engineering Kang, Joonkoo ; University of Michigan, Material Science and Engineering, Chemical Engineering, Chemistry, Biomedical Engineering, Macromolecular Science and Engineering Roccio, Marta; University of Bern, Inner Ear Research, Department of Clinical Research lellouche, jean paul; Bar-Ilan University, Department of Chemistry, Nanomaterials Research Center, Institute of Nanotechnology & Advanced Materials
Subject area & keyword:	Biomedical < Biological

Conductive Hybrid Carbon Nanotube (CNT)-polythiophene coatings for Innovative Auditory Neuron-Multi-Electrode Array Interfacing

Ostrovsky S.,[1] Hahnewald S.,[2] Kiran R.,[3] Mistrik P.,[3] Hessler R.,[3] Tscherter A.,[4] Senn P.,[2,5] Kang J.,[6] Kim J.,[6] Roccio M.[2*] and Lellouche JP.[1*]

1 Institute of Nanotechnology and Advanced Materials and Department of Chemistry, Bar-Ilan University, Ramat Gan 5290002, Israel

2 Inner Ear Research Laboratory, University Departments of Clinical Research and Otorhinolaryngology, Head & Neck Surgery, Inselspital, University of Bern 3010, Switzerland

3 MED-EL Elektromedizinische Geräte GmbH, Innsbruck 6020, Austria

4 Department of Physiology, University of Bern, Bern 3012, Switzerland

5 Department of Clinical Neurosciences, Service of Otorhinolaryngology, Head & Neck Surgery, University Hospital of Geneva (HUG), Geneva 1205, Switzerland

6 Chemical Engineering, Chemistry, Biomedical Engineering, Macromolecular Science and Engineering, University of Michigan, Ann Arbor, Michigan 48109, USA

*shared last author contribution

Abstract

Cochlear implants (CIs) are neuroprosthetic devices that restore hearing in deaf patients. They consist of a linear electrode array surgically inserted into the scala tympani of the cochlea. In this position the array directly stimulates the spiral ganglion neurons (SGNs), bypassing lost or nonfunctioning sensory hair cells. In order to reduce the energy needed to stimulate the SGNs, we attempted to improve the conductivity between the electrode CI by creating conductive nanocomposites. We assessed the functional modification of CI platinum (Pt) pads by using multi-walled carbon nanotubes (MWCNTs) either alone or in combination with a conductive polythiophene phase, to obtain conductive nanocomposites (NCs). A novel functional *poly*($EDOT_3$:$EDOT\text{-}COOH_1$) copolymer was synthesized by liquid-phase oxidative polymerization (LPP) of both 3,4-ethylenedioxythiophene (EDOT) and carboxylated EDOT (EDOT-COOH) monomers. Molar ratios of monomers $EDOT_3$:$EDOT\text{-}COOH_1$ were obtained and a *poly*($EDOT_3$:$EDOT\text{-}COOH_1$) polymeric phase was further incorporated with oxidized MWCNTs (ox-MWCNTs) to obtain a homogeneous conductive NC phase. Immobilization of single components or NC onto Pt electrodes using cysteamine-based covalent modification has been achieved and characterized. Impedance spectroscopy of Pt-modified electrodes showed a reduced resistance at different frequencies for the specific NC consisting of *poly*($EDOT_3$:$EDOT\text{-}COOH_1$)/SH/ox-MWCNTs/SH (1:1 wt%). Finally, we revealed the functional outcome of these nanostructured chemical modifications concerning the stimulation of SGN *in vitro* using multi-electrode arrays (MEAs). We aimed at reducing the energy needed to stimulate the SGNs and obtain an effective neuronal response. This has been observed for Pt electrodes modified with NC.

List of abbreviations

CIs: Cochlear Implants

SGNs: Spiral Ganglion Neurons

Pt: Platinum

MWCNTs: Multi-Walled Carbon Nanotubes

NCs: nanocomposites

EDOT: 3,4-ethylenedioxythiophene

MEAs: Multi-Electrode Arrays

1. Introduction

The cochlear implant (CI) has become the gold standard in the treatment of children and adults with congenital or acquired deafness [1]. This neuroprosthesis consists of an electrode array surgically inserted into the cochlea in order to directly stimulate the spiral ganglion neurons (SGNs). Because of its complexity, it has to meet high standards, particularly in terms of the biocompatibility and conductivity of the CI surface components [2]. In order to achieve the best surface modification of the microelectrode array, it is necessary to find new materials and technologies to fabricate microelectrodes that will be useful for recording, and stimulation.

Conductive polymers (CPs) can be used for the nanofabrication of metal contacts in microelectrode arrays and in the case of CIs potentially offer the benefit of improving their mechanical and electrical properties [3]. A unique advantage of conducting polymers is that various substances can be doped into the polymer matrix for different purposes, including decreasing the interface impedance [4, 5] and improving the adhesion and extension of neurons on the surface of electrodes [6, 7]. CPs have been utilized for coating metallic electrodes and have displayed excellent performance delivering charge in the neuroprosthetic interface [3, 8, 9]. Of the conducting polymers, poly(3,4-ethylenedioxythiophene) (PEDOT) has been extensively studied because of its superior conductivity, biocompatibility and enhanced strain match with soft tissue [10, 11]. Previous reports have indicated that PEDOT possesses superior electrochemical stability [12] and high sensitivity to the electrode surface as a result of its increased surface to volume ratio [9, 13].

However, in most studies, *in situ* electrochemical polymerization of PEDOT films for use as microelectrode coatings is carried out [14-16]. In this study we develop a novel method for the production of microelectrode coatings using simple covalent attachment of the polymer nanocomposite. A strong covalent binding of the polymer may improve the durability and reversibility of the microelectrode array surface coatings. To generate a polymer with functional surface chemistry, it is possible to modify the chemical structure of the 3,4-ethylenedioxythiophene (EDOT) monomer [11, 17] and to copolymerize two or more suitably functionalized monomers to obtain conducting polymers with properties intermediate to those of the individual polymers [18]. Among these functional groups, carboxylic acids provide a particularly facile means of functionalizing monomers [19]. We have therefore utilized a simple carboxylic acid functionalized carboxylated EDOT (EDOT-COOH) monomer chemically polymerized with EDOT unit monomer, (1:3) molar ratios respectively. Thus, the inclusion of a carboxylic acid functional group enables the generation of copolymer coatings, thereby manipulating the surface concentration of the COOH groups and their chemical modifications with organic molecules. Correspondingly, a newly synthesized conductive copolymer *poly*($EDOT_3$:$EDOT\text{-}COOH_1$) was used as the electrode

modification material in this study. In order to enhance the electroactivity of neural electrodes, we doped chemically functionalized oxidized multi-walled carbon-nanotubes (MWCNTs) into the corresponding conducting copolymer matrix.

Recent investigations have begun addressing the issue of the effects of conducting polymers and carbon nanotube (CNT) substrates on neural growth [8, 20].

CNTs provide an excellent nanoscale tool to improve neuron-electrode coupling efficiency [17, 21] due to various surface properties such as polarity, roughness, chemistry and charge [18, 19, 22, 23].

In this study, for the first time, we report the chemical covalent attachment of the novel hybrid nanocomposite containing conductive *poly*($EDOT_3$:$EDOT\text{-}COOH_1$) copolymer embedded with oxidized MWCNTs on the platinum (Pt) microelectrode array surface of the cochlear implants. We compare the functionalization of the Pt microelectrode array surface with three types of coatings: (i) sole oxidized MWCNTs (ox-MWCNTs), (ii) sole copolymer *poly*($EDOT_3$:$EDOT\text{-}COOH_1$) and (iii) the corresponding novel hybrid conducting nanocomposite *poly*($EDOT_3$:$EDOT\text{-}COOH_1$)/ox-MWCNTs at a 1:1 wt% ratio. It has been shown that the novel hybrid nanocomposite can reduce impedance and increase the capacitive nature of current conductance over Faradaic charge transfer. This can help to further minimize potential harm to cochlear tissue caused by electrical stimulation of the CI electrode array [24, 25]. Furthermore, we demonstrate successful extracellular activity of primary auditory neurons (SGNs) testing with sole oxidized MWCNTs (ox-MWCNTs) or the hybrid *poly*($EDOT_3$:$EDOT\text{-}COOH_1$)/oxMWCNTs nanocomposite implemented on multi-electrode arrays (MEAs). We have previously assessed the possibility of analyzing SGN electrode interfaces on MEAs [26]. Here, we demonstrate that this platform is also suitable for a systematic assessment of any electrode surface modification. We have found that, indeed, chemical modifications of Pt electrodes with the hybrid nanocomposite *poly*($EDOT_3$:$EDOT\text{-}COOH_1$)/ox-MWCNTs and modified MWCNTs have significantly improves recordings of SGN activity and resulted in a reduced threshold required for effective electrode-induced SGN stimulation.

2. Experimental section

2.1 Characterization

All reagents were obtained commercially from Sigma-Aldrich unless otherwise noted. The MWCNTs used in this work have been purchased from Amorphous Materials, Inc. (NanoAmor). They are characterized by a purity of 95%, an average external diameter of 8-15 nm, a length of 10-50 μm and a surface area of 233 m^2/g. X-ray photoelectron spectroscopy (XPS), Fourier-transform

infrared (FTIR) and thermogravimetric (TGA) analyses required the preparation of dry powder samples (vacuum stove for 1 h at 40°C followed by lyophilization using a FreeZone 2.5-liter bench-top freeze-dry system – Labconco, Kansas City, MO, USA). FTIR spectra were recorded using a Bruker TENSOR 27 spectrometer (Diffuse Reflectance Accessory EasyDiff, PIKE Technologies, 4cm1 resolution). Samples were prepared by Mixing nanoparticle (NP) powders with dry IR grade KBr (2% weight). High-Resolution Scaning Electron Microscop HR-SEM images were taken using an FEI, Helios 600 device. Quantification of polymer amounts *via* temperature-dependent weight loss was evaluated by thermogravimetric analysis (TGA), Thermo-finnigan TAQ600-0348, model SDT Q600) using a temperature profile of 50-800°C at 10°C/min (N_2 atmosphere).

2.2 Chemical synthesis of the *poly*(EDOT$_3$:EDOT-COOH$_1$)

Fe(III) p-toluenesulfonate hexahydrate oxidant ($Fe(OTs)_3$, 4.06 g, 6.0 mmol), imidazole (0.0.66 g, 6.0 mmol) as a weak base and EDOT monomer (0.5 g, 3.0 mmol) solutions were prepared at a 2:2:1 molar ratio in methanol (MeOH) (separate flasks) by stirring 1-2 minutes at RT. EDOT and EDOT-carboxylic acid (EDOT-COOH, 0.18 g, 1.0 mmol) were then added to the weak base solution flask and subsequently added to the $Fe(OTs)_3$ MeOH solution. The mixture was refluxed at 110°C for 2 h. Following the reaction, the solvent was evaporated under reduced pressure. The resultant residual copolymer *poly*(EDOT$_3$:EDOT-COOH$_1$) as a black powder was then washed by centrifugation (13,000 rpm, 10 min) in a 1/1 v/v MeOH/H_2O mixture for three cycles.

2.3 Impedance spectroscopy

Impedance spectroscopy (IS) was carried out to determine the frequency dependence of impedance. Measurements were performed before and after nanomaterial deposition using a Bio-Logic potentiostat controlled by an EC-Lab® platform. Measurements were made in a saline solution using a sinusoidal stimulus with Vpp = 20 mV.

2.4 Spiral ganglion explant preparation

5-8 day-old mice pups (C57/Bl6) were used for the study. The protocol was approved by the local animal welfare authority (BE117/12, Amt für Landwirtschaft und Natur des Kantons Bern, Switzerland) and all experiments were carried out according to ethical guidelines. Otic capsules were isolated from the skull and transferred into cold Hank`s Balanced Salt Solution (HBSS) (Invitrogen, USA) for further dissection under a binocular dissection microscope (Nikon SMZ100, Japan). The cochleae were dissected and the surrounding bone removed. The stria vascularis and the organ of Corti were removed consecutively. Finally, the spiral ganglions (SGs) were isolated. SG explants (3 to 4 explants with a dimension of 200-500 μm) were cut from the SG and plated on

MEA coated with Matrigel™ (Corning, USA) diluted in 1:10 Neurobasal medium: Neurobasal (Invitrogen, USA), B27 (Invitrogen, USA), HEPES (Invitrogen, USA), Glutamax (Invitrogen, USA), Ampicillin (Sigma, USA), 10% fetal bovine serum (FBS) (Invitrogen, USA) and 5 ng/ml brain-derived neurotrophic factor (BDNF, R&D Systems, USA).

2.5 Multi-electrode array setup

MEA slides (Qwane Biosciences, Lausanne, Switzerland) containing 68 platinum electrodes of dimensions 40 μm x 40 μm, an inter-electrode distance of 200 μm and an estimated impedance of 400KΩ/1KHz were used. MEAs contain four large ground electrodes that are placed around the recording site. A custom-made setup was used to amplify and digitize the electrical signals of the electrodes [27]. Spontaneous activity was recorded for a minimum of 5 minutes. Successful active cultures were defined as MEA experiments showing activity from at least one of the 68 electrodes. Electrodes showing a minimum activity of 0.1 single unit potential (SUP) per second were defined as spontaneously active. Tetrodotoxin (TTX, Alomone Labs, Israel) was used at a concentration of 1 μM to block voltage-gated sodium channels in order to define the background noise as previously described [26]. For electrical stimulation of the culture, monopolar biphasic stimuli (with a total duration of 80 microseconds) were applied *via* one of the electrodes, and the responses from the remaining ones were recorded. The stimuli were current-controlled using a stimulator (Multi Channel Systems Stimulator STG 2008). Stimulation was performed manually with 10 consecutive pulses. Only electrodes responding with an action potential in at least 7 out of 10 stimulations were defined as responding electrodes and further analyzed as previously described [26]. Custom-made Labview software (National Instruments, Switzerland) was used to control the A/D card (NI-DAQ-card, AT-MIO-64E-3, National Instruments, Switzerland). Data were digitized at a rate of 6 kHz with 12-bit resolution and stored on a hard disk for offline analysis [27]. To identify current thresholds for each modification, pairs of neighboring electrodes were chosen, in which one electrode was used for stimulation and the other for recording. We first identified the responding electrodes using electrical current parameters typical of CI stimulation: a biphasic pulse with a duration of 40 μs per phase and 80μA amplitude [28].

2.6 Immunostaining and neuronal cultures on MEA

Samples were fixed with 4% paraformaldehyde for 10 min and washed three times with PBS, then permeabilized for 5 min with 0.01% Triton-X-100 in PBS and incubated with 4% BSA in PBS (with 0.001% Triton-X-100) for 2 hours. Samples were stained for 1:200 TUJ (R&D Systems, USA) incubated overnight at 4°C. Secondary fluorescently-labeled antibody (anti mouse-Alexa

Fluor 488), diluted 1:500 in PBS (with 4% BSA + 0.001% Triton-X-100), was left for 2 hours at 4°C. Cultures were analyzed using a Leica DMI4000 B microscope (Leica Microsystems, Germany) equipped with CCD cameras (DFC425 C and DFC360 FX, both Leica Microsystems, Germany).

2.7 Statistical analysis

Unpaired Student's t-tests were performed using Grey Pt as a reference (black bars). Analysis was performed using Graph Pad Prism 6 (GraphPad Software, La Jolla, CA 92037 USA). Data are shown as mean +/- standard error of the mean (SEM). Significance was labeled "ns" for "not significant", and $p<0.05$ was marked by "*".

3. Results and discussion

3.1 Oxidative polymerization of EDOT and EDOT-COOH monomers

Conducting copolymer was obtained from mixtures of the two monomers containing EDOT and EDOT-COOH with 3:1 mole fractions, respectively. For the oxidative copolymerization in solution, we chose to use the conducting oxidant type Fe(III) toluenesulfonate (OTs^-), due to its counter-anion property that is critical for optimal polymer doping/conductivity [13, 29]. The experimental procedure for an oxidative polymerization of both EDOT and EDOT-COOH monomers is described in **Scheme 1**.

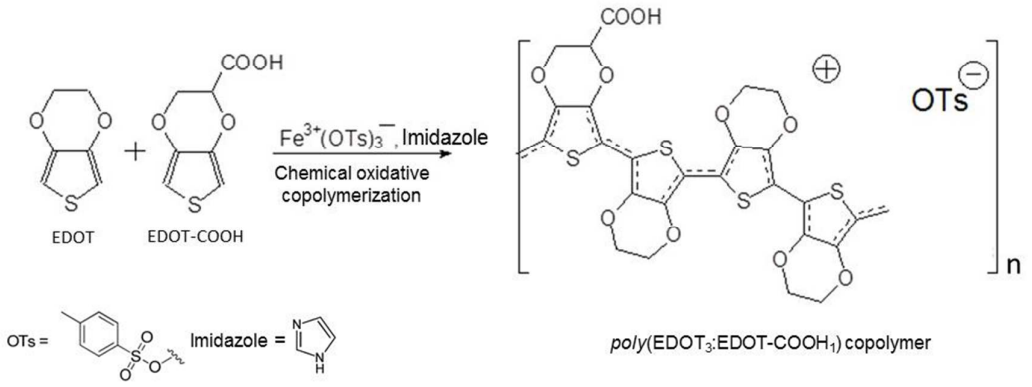

Scheme 1: Chemical oxidative copolymerization of EDOT and EDOT-COOH.

The obtained *poly*($EDOT_3$:EDOT-$COOH_1$) was then characterized by FTIR spectroscopy (Fig.1). The characteristic peaks for carboxylic acid groups (C = O modes) appeared at 1723.54 cm^{-1} [30]. Peaks that appeared at 1573.18 and 1462.45 cm^{-1} are stretching modes of both C = C and C-C bonding for the copolymer thiophenyl ring. Stretching modes of the ethylenedioxy group appeared at 1269.43 and 1120.60 cm^{-1}, while the peak around 900 cm^{-1} is due to the ethylenedioxy ring deformation mode within the copolymer. Interestingly, former thiophenyl ring C-H bending modes at 889.60 cm^{-1} disappeared in the polymer spectrum, demonstrating the formation of 2,5-substituted copolymer chains.

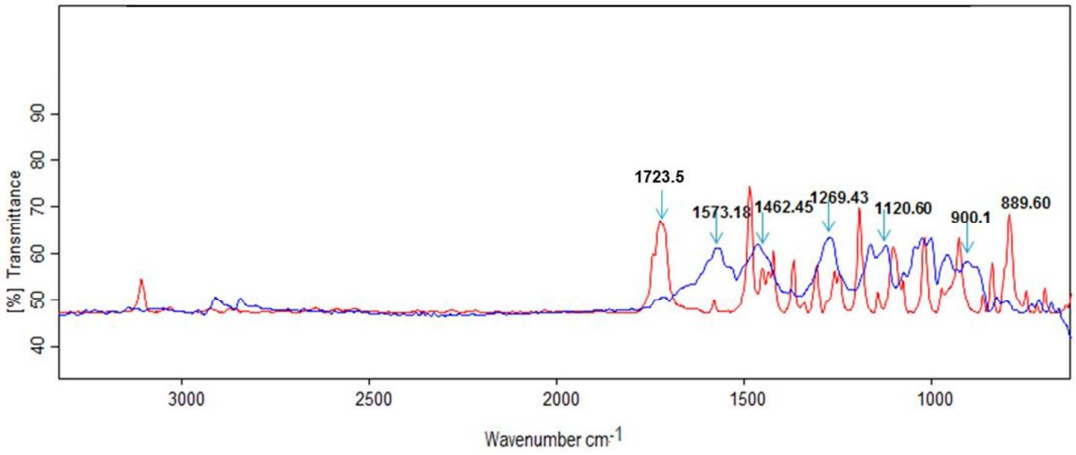

Figure 1: FTIR spectrum of the bare EDOT-COOH (red line) and the copolymer *poly*($EDOT_3$:EDOT-$COOH_1$) (blue line).

Furthermore, TGA was performed to confirm and characterize the preparation of the conductive copolymer phase (Fig. 2). For bare EDOT thermogram, there is a slight (17%) decrease in weight at 350°C (green line). In contrast, the *poly*($EDOT_3$:EDOT-$COOH_1$) copolymer (blue line) showed a 49.17% decrease in weight of the analyzed material at 357°C. This accounts for the significant increase observed in the nanocomposite organic content after the polymerization step. The slight weight loss in EDOT (green curve) observed at 100°C may be due to H_2O/volatile desorption and elimination.

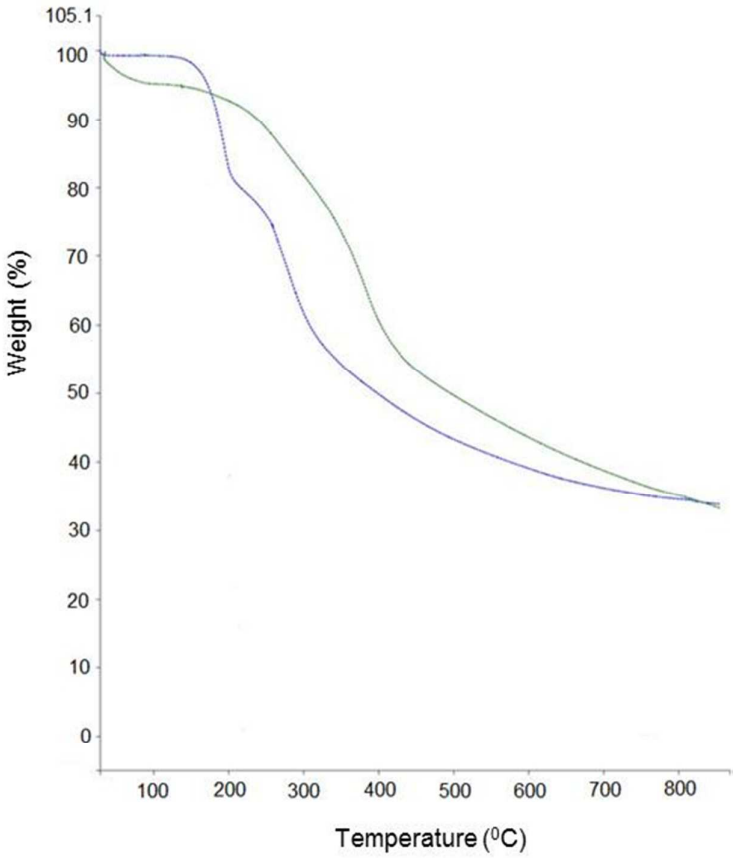

Figure 2: TGA curves for bare EDOT monomer (green line) and *poly*($EDOT_3$:EDOT-$COOH_1$) (blue line).

To quantify the outer carboxylic acid groups accessible for chemical modifications on the surface of the *poly*($EDOT_3$:EDOT-$COOH_1$) phase, Kaiser test was performed (a highly sensitive analytical UV spectroscopic Kaiser test) [23]. Triplicate measurements provided an average value of 0.1 mmol of COOH groups per gram of *poly*($EDOT_3$:EDOT-$COOH_1$).

3.2 Oxidation of MWCNTs

The chemical oxidation of corresponding MWCNTs has been optimised using statistically significant design-of-experiments methods (DOE) [26]. The brief procedure is as follows: MWCNTs (50 mg) are suspended in a 3:1 mixture of concentrated H_2SO_4 and HNO_3 (24 mL) by bath ultrasonication for 20 minutes at RT. Then the mixture is magnetically stirred and heated at 50°C for 24 h. It is subsequently diluted with deionized water (50 ml) and centrifuged (12000 rpm, 20 min) to afford end-opened ox-MWCNTs. This treatment provides carboxylic acid groups (defects) onto the MWCNT surface as well as at the open ends. Carboxyl modifications on MWCNT

surfaces increase the solubility of ox-MWCNTs in organic solvents and water [26]. Elemental analyses of ox-MWCNTs afford specific atomic percentage values of C, O and H elements (Table 1) for oxidation tracking. Triplicate measurements of the Kaiser test provided an average value of 0.157 mmol/g of COOH groups of ox-MWCNTs.

3.3 Chemical modification of ox-MWCNT and *poly*($EDOT_3$:$EDOT\text{-}COOH_1$) copolymer with cysteamine

A partial chemical modification (50% of the amount of accessible COOH groups of ox-MWCNTs and *poly*($EDOT_3$:$EDOT\text{-}COOH_1$), Kaiser test measurement) was performed using cysteamine to produce a bi-functional polyCOOH/polySH phase for further coating of the multi-electrode Pt array interface based on strong HS-Pt atoms interactions.

3.3.1 Chemical modification of ox-MWCNTs with cysteamine-enabling Pt electrode coating

Ox-MWCNTs (100.0 mg) were dispersed in THF (10 mL) by low-power bath sonication (30 min, bath sonicator), and CDI (carbonyldiimidazole, 1.3 mg, $7.85*10^{-3}$ mmol) was then added to the resulting dispersion and mixed for 2 h at RT. Cysteamine (0.6 mg, $7.85*10^{-3}$ mmol) was then added to the ox-MWCNT dispersion for 24 h at RT under stirring. The cysteamine-modified ox-MWCNTs were then washed with 1/1 v/v ddH_2O/MeOH using centrifugation (10 min, 10,000 rpm, 0°C) yielding cleaned thiolated ox-MWCNT/SH phases.

3.3.2 Chemical modification of the *poly*($EDOT_3$:$EDOT\text{-}COOH_1$) copolymer with cysteamine-enabling Pt electrode coating

poly($EDOT_3$:$EDOT\text{-}COOH_1$) (100mg) was dispersed in ethanol (10 mL) by low-power bath sonication (30 min, bath sonicator), and EDC (1-Ethyl-3-(3-dimethylaminopropyl) carbodiimide, 0.958 mg, $5*10^{-3}$ mmol) was then added to the resulting dispersion and mixed for 2 h at RT. Cysteamine (0.385 mg, $5*10^{-3}$ mmol) was added to the resulting dispersion for 24 h at RT under stirring. Next, the cysteamine-modified *poly*($EDOT_3$:$EDOT\text{-}COOH_1$) was washed with ddH_2O using centrifugation (10 min, 10,000 rpm, 0°C), yielding a clean thiolated *poly*($EDOT_3$:$EDOT\text{-}COOH_1$)/SH phase.

Elemental analyses of both *poly*($EDOT_3$:$EDOT\text{-}COOH_1$)/SH and ox-MWCNT/SH afforded corresponding atomic percentage values for C, O and H elements and also for thiol (S element) and nitrogen (N element) tracking (Table 1). Interestingly, the presence of both S and N signals confirmed the expected elemental composition of thiolated ox-MWCNTs/SH and the copolymer.

Importantly, the S element was detected for thiolated composites while it was not observed for starting materials (data not shown).

	XPS (atomic concentration, %)				
Sample	C	H	N	O	S
ox-MWCNT	48.58	6.02	-	42.32	-
ox-MWCNT/SH	48.79	3.36	1.46	45.07	1.32
poly($EDOT_3$:EDOT-$COOH_1$)	64.95	5.26	-	21.13	6.42
poly($EDOT_3$:EDOT-$COOH_1$)/SH	61.21	7.58	2.72	20.06	8.43

Table 1. XPS elemental composition of oxidized MWCNTs (ox-MWCNT), MWCNT modified with cysteamine (ox-MWCNT/SH), *poly*($EDOT_3$:EDOT-$COOH_1$) and copolymer modified with cysteamine *(poly*($EDOT_3$:EDOT-$COOH_1$)/SH.

3.3.3 Incorporation of ox-MWCNT/SH into a *poly*($EDOT_3$:EDOT-$COOH_1$)/SH copolymer matrix

In order to functionalize the electrode Pt surface with an innovative conductive nanocomposite, ox-MWCNT/SH and *poly*($EDOT_3$:EDOTCOOH$_1$)/SH (1:1 wt%) were dispersed in methanol using mild bath ultrasonication (20 minutes, RT) to afford a stable and homogeneous *poly*($EDOT_3$:EDOT-$COOH_1$)/SH/ox-MWCNT/SH suspension**.** Since the *poly*($EDOT_3$:EDOTCOOH$_1$) structure usually has conjugated heterocyclic π bonds, strong interactions between both copolymer chains and MWCNT sidewalls should arise from both π-π stacking and van der Waals forces. After mixing, the solvent was evaporated under reduced pressure and the corresponding nanocomposites (NCs) were dried in vacuum (38°C, $1*10^{-2}$ atm) overnight to afford clean *poly*($EDOT_3$:EDOTCOOH$_1$)/SH/ox-MWCNT/SH phases.

4. Functionalization of multi-electrode arrays (MEAs)

The thiol-mediated multivalent grafting afforded the requested microelectrode coating *via* multivalent Pt-S quasi-covalent bonding/multiphase anchoring. MEAs were coated with (i) sole sidewall-modified oxidized ox-MWCNTs/SH, (ii) sole copolymer *poly*($EDOT_3$:EDOT-$COOH_1$)/SH and (iii) a deposition of the nanocomposite *poly*($EDOT_3$:EDOT-$COOH_1$)/SH/ox-MWCNTs/SH (1:1

wt%). Next, microelectrode arrays were rinsed with ethanol (30 ml), dried under a nitrogen flow and then immersed in a MeOH solution containing 1.0 mg/mL of the coating phases mentioned above. Argon gas was bubbled for 3 minutes (for O_2 removal) in a contacting medium. Samples were then reacted/incubated overnight using an orbital shaker (deposition cycle). After three similar deposition cycles, corresponding MEA samples were washed in EtOH three times at room temperature and dried using a dry N_2 flow.

4.1 Surface analysis of coated MEAs

Structure and characterization of the Pt surface covalent coating were obtained using HR-SEM images and elemental EDX analysis. The surface morphology of *poly*(EDOT$_3$:EDOT-COOH$_1$)/SH, ox-MWCNTs/SH and the nanocomposite *poly*(EDOT$_3$:EDOT-COOH$_1$)/SH/ox-MWCNTs/SH is represented in Fig. 3a-3c, respectively.

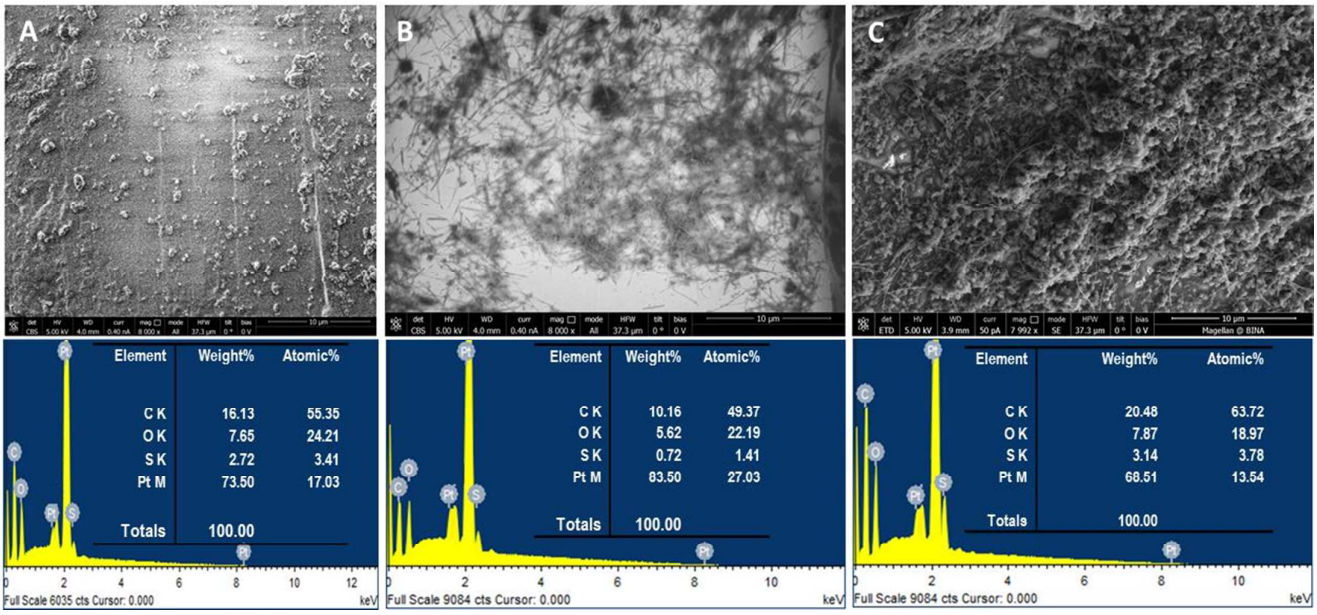

Figure 3: HR-SEM images and EDX analysis of covalently coated MEAs. **A**: Pt surface coated with *poly*(EDOT$_3$:EDOT-COOH$_1$)/SH, **B,**: Pt surface coated with ox-MWCNT/SH, **C,***:* Pt coated with nanocomposite *poly*(EDOT$_3$:EDOT-COOH$_1$)/SH/ ox-MWCNT/SH.

It is clear from these images that the morphology of the coated electrodes significantly changes when MWCNTs are doped in the copolymer matrix (Fig. 3c). The morphology of sole *poly*(EDOT$_3$:EDOT-COOH$_1$)/SH is granular in nature, with visible aggregation of the grains into clusters. These clusters, which are approximately 0.5 μm in diameter, are not uniformly coated over the Pt surface. When comparing two specific microphotographs of Pt electrode coatings with the nanocomposite *poly*(EDOT$_3$:EDOT-COOH$_1$)/SH/ox-MWCNTs/SH and sole ox-MWCNTs/SH, it is clear that increasing amounts of the polymer content improve both roughness and

distribution/homogeneity of the coating on the surface of the Pt electrode. Ox-MWCNTs/SH are distributed throughout the copolymer layer and the novel nanocomposite has a rough and porous morphology. Rough surfaces are known to promote cell growth better than smooth ones, and therefore a very rough electrode surface is desirable[24, 25]. Interestingly, EDX analysis of the ox-MWCNT/SH-coated Pt surface showed S peaks arising from the thiol atoms presented in cysteamine and covalently bound to the Pt surface. Also, no metallic contaminations of ox-MWCNTs/SH were presented because of the oxidation treatment performed on the bare MWCNTs (Fig. 3b).

5. Impedance characterization of modified electrodes

The electrode surfaces were additionally characterized by impedance spectroscopy. Here, both the amplitudes and the phase angle of the impedance were quantified as a function of frequency over the 1 to 100 kHz range. Bode plots were obtained for all three covalent coatings: ox-MWCNTs/SH, *poly*($EDOT_3$:EDOT-$COOH_1$)/SH and *poly*($EDOT_3$:EDOT-$COOH_1$)/SH/ox-MWCNTs/SH (Fig. 4**)**.

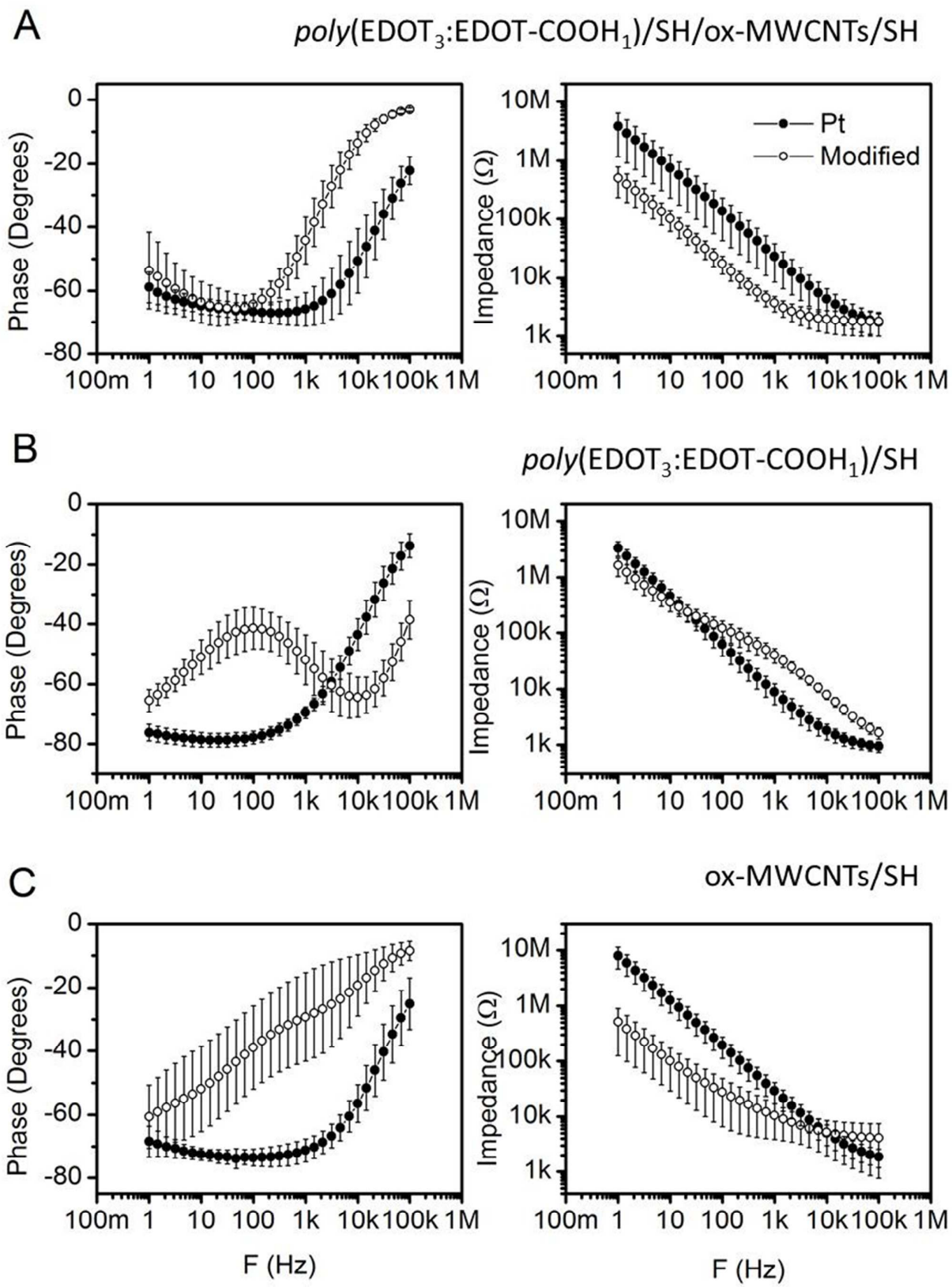
A
poly(EDOT3:EDOT-COOH1)/SH/ox-MWCNTs/SH
Phase (Degrees)
0
-20
-40
-60
-80
Impedance (Ω)
10M
1M
100k
10k
1k
Pt
Modified
100m 1 10 100 1k 10k 100k 1M
B
poly(EDOT3:EDOT-COOH1)/SH
C
ox-MWCNTs/SH
F (Hz)

Figure 4: Bode plots of Pt electrode surfaces. **A**: *poly*($EDOT_3$:EDOT-$COOH_1$)/SH/ox-MWCNT/SH , **B**: *poly*($EDOT_3$:EDOT-$COOH_1$)/SH and **C**: ox-MWCNT/SH. Each panel shows the values obtained with coated and uncoated platinum electrodes (○ and ●, respectively). Left column shows the phase of impedance, while the right column the amplitude.

The values were obtained by averaging 10 samples. Despite some variability, direct comparison with uncoated platinum surfaces indicates that the desired reduction in impedance amplitude is obtained for ox-MWCNTs/SH and the nanocomposite *poly*($EDOT_3$:EDOT-$COOH_1$)/SH/ox-MWCNTs/SH, but not for the sole copolymer *poly*($EDOT_3$:EDOT-$COOH_1$)/SH. The effect was largest in the frequency range up to 10 kHz. For example, at 10 Hz, the frequency relevant for the MEA measurements with explanted SGNs, the impedance of the Pt electrodes was reduced by a factor of 8 with both ox-MWCNTs/SH and nanocomposite *poly*($EDOT_3$:EDOT-$COOH_1$)/SH/ox-MWCNTs/SH coatings (summarized results Table 2). Such a reduction can explain the increased excitability of the primary auditory neurons (SGNs) observed by the MEA measurements. The effect grew smaller as the frequency increased. At 1 kHz, the impedance of the electrodes modified with *poly*($EDOT_3$:EDOT-$COOH_1$)/SH/ox-MWCNTs/SH was reduced by a factor of 5 and of those modified with ox-MWCNTs/SH by a factor of 2 compared to uncoated Pt surfaces (Table 2). As this frequency range is used in clinical CI devices for diagnostic recording from the primary auditory neurons, the reduced impedance can increase the battery-life of the device – an important benefit for implant users. The relevance for CI stimulation is smaller, due to the high frequency range used [28]. At 46 kHz, the upper limit of CI stimulation, no improvement in impedance amplitude is observed (Table 2).

	Electrode	**Amplitude**(kΩ)	**Phase**(degree)
1Hz	bare Pt	19.8 ± 13.8	-69.1± 3.3
	poly($EDOT_3$:EDOT-$COOH_1$)/SH/ox-MWCNTs/SH	3.7 ± 1.1	-44.2 ± 7.4
	poly($EDOT_3$:EDOT-$COOH_1$)/SH	40.1 ± 5.8	-51.9 ± 8.3
	ox-MWCNTs	10.5 ± 0.8	-47.0 ± 12.3
10Hz	bare Pt	799.8 ± 531.4	-73.3 ± 6.1
	poly($EDOT_3$:EDOT-$COOH_1$)/SH/ox-MWCNTs/SH	100.5 ± 38.9	-63.7 ± 6.5
	poly($EDOT_3$:EDOT-$COOH_1$)/SH	357.7 ± 116.4	-51.0 ± 5.7
	ox-MWCNTs	100.9 ± 71.7	-51.9 ± 13.4
46Hz	bare Pt	1.8 ± 0.9	-28.1 ± 9.0
	poly($EDOT_3$:EDOT-$COOH_1$)/SH/ox-MWCNTs/SH	1.8 ± 0.8	-4.6 ± 0.9
	poly($EDOT_3$:EDOT-$COOH_1$)/SH	2.5 ± 0.5	-52.7 ± 6.1
	ox-MWCNTs	4.3 ± 3.3	-10.780 ± 4.27

Table 2: Summarized results for amplitude and phase angle values at 1, 10 and 46 Hz.

Importantly, the surface coatings also changed the frequency dependence of the impedance phase angle (Fig. 4). In this case, ox-MWCNTs/SH and the nanocomposite *poly*($EDOT_3$:EDOT-$COOH_1$)/SH/ox-MWCNTs/SH had a large effect which shifted the phase to less negative values over the entire frequency range. The phase angle values at frequencies 1, 10 and 46 kHz are summarized in Table 2. Large shifts at 1 and 46 kHz are observed for *poly*($EDOT_3$:EDOT-$COOH_1$)/SH/ox-MWCNTs/SH (about 24° and 23.5°, respectively). The reduction in negative value of the phase angle indicates a shift towards the desired capacitive nature of the current conductance [27]. To determine the underlying change in the double-layer capacitance (Q) responsible for such a shift, the Bode plots of amplitude and phase were fitted simultaneously into a mathematical R(QR) model of the electrode-electrolyte interface, allowing the separation and determination of the resistive (R) and double-layer capacitance (Q) components of the impedance. The mean value for the double-layer capacitance Q of the untreated Pt electrode was 99±76 nF (n = 142) (Table 3). The largest increase was observed for the *poly*($EDOT_3$:EDOT-$COOH_1$)/SH/ox-MWCNT/SH coating (3±5 μF, n = 28), while for the ox-MWCNT/SH coating the increase was 0.59 ± 0.65 μF (n = 49) and for the sole copolymer *poly*($EDOT_3$:EDOT-$COOH_1$)/SH 0.51 ± 0.50 μF (n = 19). Consequently, the modification of the *poly*($EDOT_3$:EDOT-$COOH_1$)/SH/ox-MWCNT/SH resulted in a 30-fold increase in the capacitive component Q. Such a result indicates a significant improvement, since the capacitive nature of the obtained conductance is highly preferable to the Faradaic charge transfer for neural stimulation, due to safety issues associated with electron transfer from the platinum electrodes to the surrounding cochlear fluid [27]. This often irreversible process changes the oxidative/reduction state of some fluid components, including pH levels, which may have a detrimental effect on stimulated tissue and can even cause the apoptosis of neural cells [31]. Furthermore, such an increase in capacitance can widen the current charge-injection limits of 210 μC/cm^2 nominally recommended for continuous stimulation with platinum electrodes, since reduced capacitive impedance can enable more current flow without causing the hydrolyzation of water by the Faradaic current. This can, in turn, enhance the excitability of the neural tissue exposed to CI technology, which is important for more accurate encoding of speech, and can also reduce the charge transfer, thereby increasing the battery-life of the implant several-fold.

Electrode	Double layer capacitance Q (F)
Pt	99.0E-9 ± 76.9E-9
poly($EDOT_3$:$EDOT\text{-}COOH_1$)/SH/ox-MWCNTs/SH	2.6E-06 ± 5.0E-06
poly($EDOT_3$:$EDOT\text{-}COOH_1$)/SH	5.2E-07 ± 5.1E-07
ox-MWCNTs	5.9E-07 ± 6.5E-07

Table 3: Double-layer capacitance (Q) of modified and non-modified Pt electrodes determined from simultaneous fitting of Bode plots into mathematical R(QR) model of the electrode-electrolyte interface.

6. Evaluation of CNT or nanocomposite modifications on multi-electrode arrays using a gapless interface with murine spiral ganglion auditory neurons

In order to study, *in vitro*, the biological advantages of the novel Pt electrode surface covalent coating as stimulator of auditory neurons, we made use of a MEA platform that we previously developed and validated in the laboratory [32].

A MEA chip containing 68 electrodes was used, 40x40 μm in size, separated by an inter-electrode spacing of 200 μm, occupying a total area of 2.2 mm^2 (Fig. 5A). The Pt surface consists of a 150-nm-thick Pt layer (impedance: 400KΩ/1KHz). A representative picture of SGNs after 18 days in culture on such a MEA is shown in Fig. 5B. According to the output from the electrochemical results, corresponding novel nanocomposite and MWCNTs/SH had a significant improvement in electrode impedance, thus this nanocomposite was further tested on MEAs. The MEA electrode arrays have been modified either with ox-MWCNT/SH or with the *poly*($EDOT_3$:$EDOT\text{-}COOH_1$)/SH/ox-MWCNT/SH nanocomposite.

We assessed both spontaneous activity (Fig. 5C, 5D and 5E) and electrode-induced activity (Fig. 5F, 5G and 5H) in these cultures. The number of successful experiments, defined as MEA experiments, where at least one of the 68 electrodes showed activity, is reported in Fig. 4C and Fig. 4F, respectively. Coating the Pt electrode with ox-MWCNT/SH or the novel nanocomposite *poly*($EDOT_3$:$EDOT\text{-}COOH_1$)/SH/ox-MWCNT/SH led to an increase in the number of successful experiments. Additionally, we observed an increase in the number of electrodes detecting spontaneous activity (Fig. 5D) and electrode-induced activity (Fig. 5G) with both modifications, however significance was only achieved in case of ox-MWCNT/SH. We further analyzed the firing rate of neurons cultured on MEAs as well as the current threshold at which each type of electrode induced a response. No significant differences were observed concerning the firing rate of neurons on MEAs (Fig. 5E), indicating that intrinsic SG neuronal activity is not affected by this modification. Finally, we analyzed ca. 20 independent electrode pairs, using six different

experiments. Briefly, one electrode of the pair was used for stimulation and the second for recording. Stimulus amplitude was lowered in 5 μA steps until the responding electrode failed to detect neuronal activity. The supra-threshold level was then reported for each electrode. Unmodified Pt electrodes displayed a significantly higher threshold than most of the other electrodes (50.24μA ± 5.3). Introducing the nanocomposite coating onto the same Pt electrode enabled the reduction of the energy needed for neuronal stimulation (39μA ± 2). While a statistically significant decrease in the threshold level was observed for ox-MWCNT/SH-modified electrodes (Fig. 5H). Both types of modification increase the percentage of electrodes (37% and 43.7 % compared to 14.3%) responding with a current threshold below 30 μA considered low for our culture type [32] .

MEA electrodes, which are small (40x40 μm and up to 7x7 μm), designed to achieve high spatial resolution, have the drawback of having relatively high specific impedance. Increasing the surface-to-area ratio of the electrode, as shown here with the two surface modification, allows for a significant reduction in impedance and background noise [33]. A higher number of responding electrodes, detecting spontaneous or stimulation-induced activity, was found in MEAs modified with MWCNT and NC. However, we did not observe any changes in intrinsic neuronal firing features after electrode modification, as reported previously [34]. Notably, no negative effects were observed on the SGN culture during the culturing (18 days).

In conclusion, novel nanocomposites may seriously improve the overall performance of currently used smooth Pt electrodes in Cis, as confirmed here through *ex vivo* tests with corresponding modified MEAs.

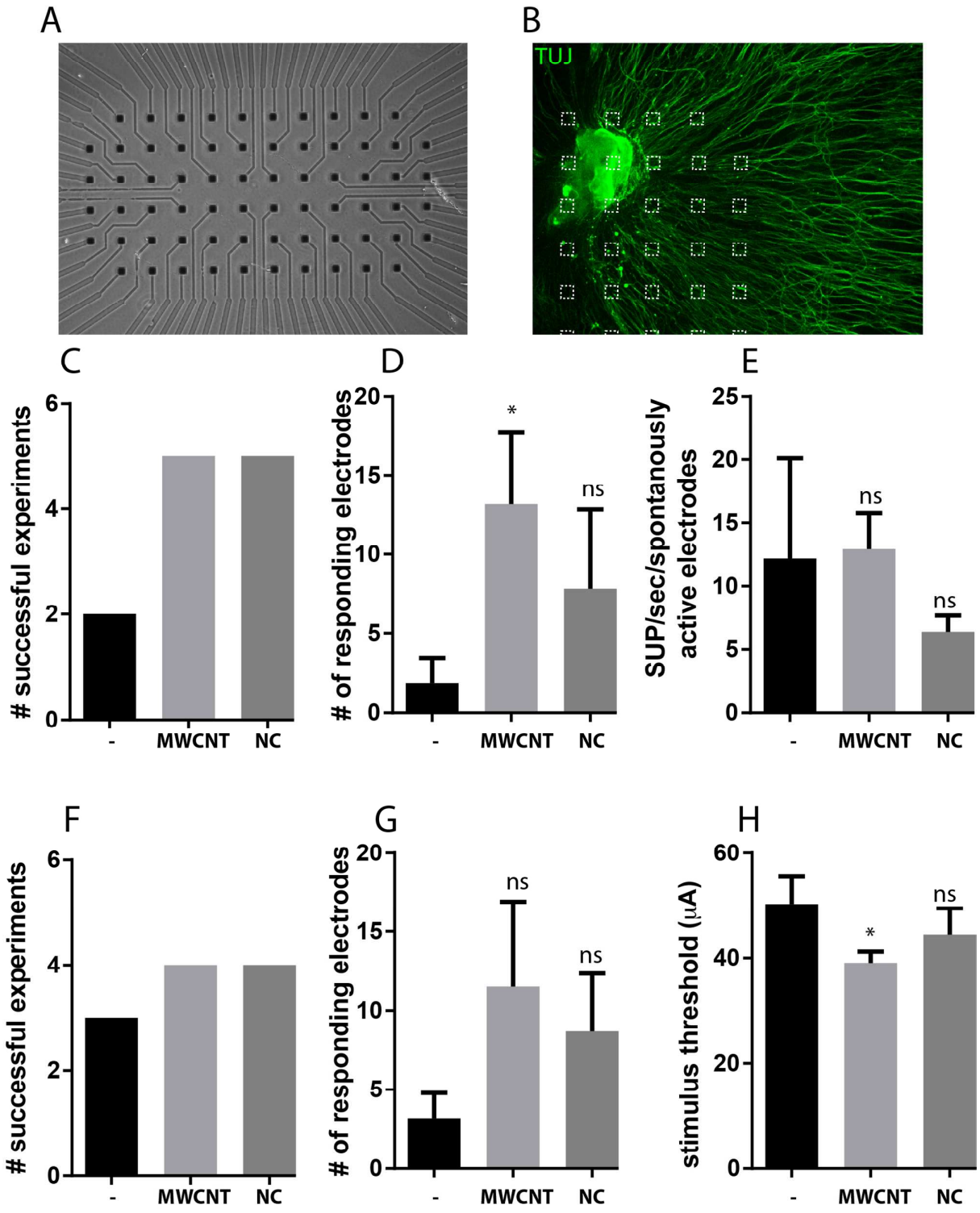

Figure 5: **A**: Image of a 68-electrode MEA used for *in vitro* study. **B**: Representative example of SGNs grown on a MEA for 18 days *in vitro*. Immunostaining for TUJ (neurons, green). Electrodes are highlighted in white dashed boxes. **C**: Number of successful MEA experiments defined as an MEA when spontaneous activity was detected on at least one of the 68 electrodes. (Total number of six experiments was performed per MEA.. **D**: Average number of electrodes detecting spontaneous activity through the six cultures. **E**:

Average firing rate per spontaneously active electrode, indicated as SUP per second/active electrode. **F**: Number of successful MEA experiments, defined as an MEA when stimulation-induced activity was detected on at least one of the 68 electrodes. **G**: Average number of responding electrodes per MEA experiment. **H**: Stimulation threshold to elicit response. 16-27 independent electrode pairs were used for the assessment. Paired t-test is performed against Pt as a reference (* = $p<0.05$, ns = not significant).

7. Conclusion

A simple covalent coating for the deposition of the *poly*($EDOT_3$:EDOT-$COOH_1$)/SH/ox-MWCNT/SH nanocomposite on micro-electrodes was devised. As for the fabrication of functional electrodes, a final conductive nanocomposite was coated on Pt electrodes *via* multivalent Pt-S quasi-covalent bonding/multiphase anchoring and was fully characterized using HR-SEM compositional analysis. Electrode roughness was found to be significantly increased by coating with a highly conductive copolymer nanocomposite. The electrochemistry data showed a very promising reduction in electrode impedance. Reduced impedance can increase the battery-life of devices, an important benefit for implant users. However, for *in vivo* application, further analysis of mechanical properties, long-term stability and possibly toxicity will have to be examined. Mechanical stability will be of particular relevance in order to avoid NC detachment during CI insertion, which could result in negative effects. We show here that a modification of Pt electrodes with nanocomposites improves the recording of SGN activity on MEAs. Interestingly, we also observed a reduction in the threshold current required to induce action-potential firing, possibly through a combination of increased electrode-neuron coupling and the reduction of impedance. The nanotechnological modification of standard Pt surfaces, as used in today's clinical cochlear implant systems and in most of the commercially available multi-electrode arrays, is a promising strategy to improve the stimulation of auditory neurons *in vitro*, and in the long term may also be used in clinical systems to lower stimulation thresholds and background noise.

Acknowledgements

Thanks to Dr. Yossi Talyossef from the Institute of Nanotechnology & Advanced Materials & the Department of Chemistry, Bar-Ilan University, Israel, for his help in the HR-SEM spectroscopy measurements. We thank Prof. Jurg Streit, Department of Physiology, University of Bern, Switzerland, for critical reading of the manuscript, scientific input and access to the infrastructure. J. Kim acknowledges financial support of the Converging Research Center Program, funded by the Ministry of Science, ICT and Future Planning (Project No. NRF-2014M3C1A8048791)". The work performed in this study is part of the NANOCI project, funded through FP7-NMP programme by the EU (Grant Agreement No.281056).

References

1. S.T. and L.T., *GMS Curr Top Otorhinolaryngol Head Neck Surg*, 2009, **8**, Doc10.
2. G. O'Donoghue, *N. Engl. J. Med.*, 2013, **369**, 1190-1193.
3. R. Green and M. R. Abidian, *Adv. Mater. (Weinheim, Ger.)*, 2015, **27**, 7620-7637.
4. M. K. Erdogan, M. Karakisla and M. Sacak, *J. Appl. Polym. Sci.*, 2015, **132**, 41979/41971-41979/41979.
5. R. Biran, D. C. Martin and P. A. Tresco, *Exp. Neurol.*, 2005, **195**, 115-126.
6. L. K. Povlich, J. C. Cho, M. K. Leach, J. M. Corey, J. Kim and D. C. Martin, *Biochim. Biophys. Acta, Gen. Subj.*, 2013, **1830**, 4288-4293.
7. R. A. Green, P. B. Matteucci, R. T. Hassarati, B. Giraud, C. W. D. Dodds, S. Chen, P. J. Byrnes-Preston, G. J. Suaning, L. A. Poole-Warren and N. H. Lovell, *J Neural Eng*, 2013, **10**, 016009.
8. M. R. Abidian, K. A. Ludwig, T. C. Marzullo, D. C. Martin and D. R. Kipke, *Adv. Mater. (Weinheim, Ger.)*, 2009, **21**, 3764-3770.
9. G. Yang, K. L. Kampstra and M. R. Abidian, *Adv. Mater. (Weinheim, Ger.)*, 2014, **26**, 4954-4960.
10. H. Zhou, X. Cheng, L. Rao, T. Li and Y. Y. Duan, *Acta Biomater.*, 2013, **9**, 6439-6449.
11. J.-W. Lee, F. Serna, J. Nickels and C. E. Schmidt, *Biomacromolecules*, 2006, **7**, 1692-1695.
12. B. Somboonsub, M. A. Invernale, S. Thongyai, P. Praserthdam, D. A. Scola and G. A. Sotzing, *Polymer*, 2010, **51**, 1231-1236.
13. Y.-H. Ha, N. Nikolov, S. K. Pollack, J. Mastrangelo, B. D. Martin and R. Shashidhar, *Adv. Funct. Mater.*, 2004, **14**, 615-622.
14. L. Sui, X. J. Song, J. Ren, W. J. Cai, L. H. Ju, Y. Wang, L. Y. Wang and M. Chen, *J. Biomed. Mater. Res., Part A*, 2014, **102A**, 1681-1696.
15. M. Heim, B. Yvert and A. Kuhn, *J Physiol Paris*, 2012, **106**, 137-145.
16. B. C. Thompson, R. T. Richardson, S. E. Moulton, A. J. Evans, S. O'Leary, G. M. Clark and G. G. Wallace, *J. Controlled Release*, 2010, **141**, 161-167.
17. Y. Xiao, X. Cui and D. C. Martin, *J. Electroanal. Chem.*, 2004, **573**, 43-48.
18. Z.-y. Zhang, Y.-j. Tao, X.-q. Xu, Y.-j. Zhou, H.-f. Cheng and W.-w. Zheng, *J. Appl. Polym. Sci.*, 2013, **129**, 1506-1512.
19. J. Y. Lee, E.-D. Jeong, C. W. Ahn and J.-W. Lee, *Synth. Met.*, 2013, **185-186**, 66-70.

20. H. H. Zhou, X. Cheng, L. Rao, T. Li and Y. W. Y. Duan, *Acta Biomater*, 2013, **9**, 6439-6449.
21. L. Bareket-Keren and Y. Hanein, *Frontiers in neural circuits*, 2012, **6**, 122.
22. E. B. Malarkey, K. A. Fisher, E. Bekyarova, W. Liu, R. C. Haddon and V. Parpura, *Nano Lett.*, 2009, **9**, 264-268.
23. E. Kaiser, R. L. Colescott, C. D. Bossinger and P. I. Cook, *Anal. Biochem.*, 1970, **34**, 595-598.
24. G. Cellot, E. Cilia, S. Cipollone, V. Rancic, A. Sucapane, S. Giordani, L. Gambazzi, H. Markram, M. Grandolfo, D. Scaini, F. Gelain, L. Casalis, M. Prato, M. Giugliano and L. Ballerini, *Nat. Nanotechnol.*, 2009, **4**, 126-133.
25. S. Schlie-Wolter, A. Deiwick, E. Fadeeva, G. Paasche, T. Lenarz and B. N. Chichkov, *ACS Appl. Mater. Interfaces*, 2013, **5**, 1070-1077.
26. M. Piran, V. Kotlyar, D. D. Medina, C. Pirlot, D. Goldman and J.-P. Lellouche, *J. Mater. Chem.*, 2009, **19**, 631-638.
27. D. R. Merrill, M. Bikson and J. G. R. Jefferys, *J Neurosci Methods*, 2005, **141**, 171-198.
28. F.-G. Zeng, S. Rebscher, W. Harrison, X. Sun and H. Feng, *IEEE Rev Biomed Eng*, 2008, **1**, 115-142.
29. Y. H. Ha, N. Nikolov, S. K. Pollack, J. Mastrangelo, B. D. Martin and R. Shashidhar, *Adv Funct Mater*, 2004, **14**, 615-622.
30. B. Somboonsub, S. Srisuwan, M. A. Invernale, S. Thongyai, P. Praserthdam, D. A. Scola and G. A. Sotzing, *Polymer*, 2010, **51**, 4472-4476.
31. U. Scarpidis, D. Madnani, C. Shoemaker, C. H. Fletcher, K. Kojima, A. A. Eshraghi, H. Staecker, P. Lefebvre, B. Malgrange, T. J. Balkany and D. W. T. R. Van, *Otol Neurotol*, 2003, **24**, 409-417.
32. S. Hahnewald, A. Tscherter, E. Marconi, J. Streit, H. R. Widmer, C. Garnham, H. Benav, M. Mueller, H. Lowenheim, M. Roccio and P. Senn, *J Neural Eng*, 2016, **13**, 016011.
33. T. Gabay, M. Ben-David, I. Kalifa, R. Sorkin, Z. e. R. Abrams, E. Ben-Jacob and Y. Hanein, *Nanotechnology*, 2007, **18**, 035201/035201-035201/035206.
34. V. Lovat, D. Pantarotto, L. Lagostena, B. Cacciari, M. Grandolfo, M. Righi, G. Spalluto, M. Prato and L. Ballerini, *Nano Lett.*, 2005, **5**, 1107-1110.